The formation of patterns in non-equilibrium growth

Eshel Ben-Jacob & Peter Garik

Crystal growth under non-equilibrium conditions can give rise to complex patterns which are generically similar to those found in processes such as viscous fingering, aggregation and electrochemical deposition. Recent theoretical understanding focuses on the interplay between the macroscopic driving force associated with the phase transition and the microscopic interfacial dynamics.

THE formation of patterns and shapes in the natural world has long been a source of fascination. Examples are many and varied, ranging from the growth of a snowflake to the aggregation of a soot particle, from oil recovery by fluid injection to solidification of metals, and from the formation of a coral reef to cell differentiation during embryonic development. The challenge is to understand the spontaneous formation of patterns from a disordered environment[1-4]. Is each of these diverse patterns the result of unique causes and effects, or are there unifying underlying principles? The past few years have seen the emergence of a rough outline of such principles. These developments offer the hope that a unified theoretical framework can be formulated to provide a coherent picture of pattern formation.

The cornerstone of these developments is the recognition that growth patterns may be determined by the interplay between microscopic interfacial dynamics and external macroscopic ('thermodynamic') forces. Most research has focused on systems in which the macroscopic dynamics are determined by a diffusion field. For such systems, the patterns that form may be grouped into a small number of typical 'essential shapes' or morphologies, observed in different systems and over many length scales (from metres to micrometres). Some examples of these (faceted[5], dendritic[4], dense-branching[6] and fractal[7-9]) are shown in Fig. 1.

The transfer of information from the microscopic to the macroscopic level is self-evident in the growth of a snowflake[10], where the sixfold symmetry of the underlying ice crystal lattice is manifest in the dendritic branches of the flake. (In the formation of real snowflakes, however, other factors such as latent heat also play a role.) How is the macroscopic form influenced by microscopic effects in this way? One can obtain a qualitative understanding by considering the dynamics of non-equilibrium growth. In a system out of equilibrium a stable phase will propagate into an unstable or metastable one. In the formation of snowflakes, for example, the stable solid phase propagates into the unstable supersaturated water-vapour phase. The rate of growth of the stable phase is limited by a diffusion process, in this case the diffusion of water molecules from the gas phase into the crystal. In this process, the kinetics of diffusion tend to drive the system towards the formation of 'decorated' and irregular shapes. Diffusion kinetics determine the macroscopic approach towards equilibrium, and influence the structures created on many length scales. By contrast, the microscopic dynamics occurring at the interface (determined by surface tension, surface kinetics and anisotropy; see Box A) are associated with microscopic length scales and are influenced by molecular-scale symmetries. The final interfacial pattern results from the interaction between the microscopic and macroscopic levels. For example, if the system is sufficiently far from equilibrium, the interface can advance so rapidly that the stable phase does not have time to reach its lowest-energy state on the microscopic level, and a metastable microstructure results. The growth of quasicrystals is an example of such a process.

Box A: Microscopic interfacial dynamics

Surface tension reflects the microscopic forces between atoms (or molecules) at an interface[4,5]. It lowers the temperature, T_i, of the curved parts of the interface according to:

$$T_i = T_m - \left(\frac{L}{C_p}\right) d_0 \kappa$$

Here L is the latent heat of the liquid–solid transition, C_p is the heat capacity of the liquid at constant pressure, T_m is the melting temperature of a flat interface, κ is the local curvature of the interface, and d_0 is the capillary length (proportional to the surface tension), typically of the order of nanometres. This equation (the Gibbs–Thompson relation) is a statement of local equilibrium for a curved interface. At local equilibrium, the free energy of the melt and the solid are the same, and there is no driving force either for melting or for solidification. For the interface to advance, there must be a degree of undercooling. We assume a linear relationship between interfacial (normal) velocity v_n and undercooling:

$$T_i = T_m - \left(\frac{L}{C_p}\right) d_0 \kappa - \left(\frac{L}{C_p}\right) \beta_0 v_n$$

The last term is meant to phenomenologically embody the microscopic dynamics of surface kinetics[15], although experimentally the relationship seems to be more complicated[48].

The effects of surface tension and surface kinetics appear (with a different functional form) in almost all non-equilibrium growth processes. For example, in the Hele-Shaw cell the pressure along the interface is given by[6,26]

$$P_i = P_a - d_0 \kappa - \beta_0 v_n^{\gamma}$$

Here P_a is the applied pressure. The 'surface kinetics' term arises from the excess pressure needed to overcome the frictional drag of the fluid against the cell plates.

The third player in the game is anisotropy[15]. The average bonding energy between atoms at the interface depends on the orientation of the interface. Hence, it costs different amounts of energy to bend the interface in different orientations. The functional dependence is characteristic of the specific system. A tractable two-dimensional form is obtained by substituting d_0 for $d_0(1 - d_1 \cos(m\theta))$, where d_1 is the magnitude of the m-fold anisotropy and θ is the angle between some fixed direction in space and the direction normal to the interface. Surface kinetics are also a function of θ: an atom will attach itself to the interface at different rates, depending on the surface orientation, leading to a similar dependence on θ.

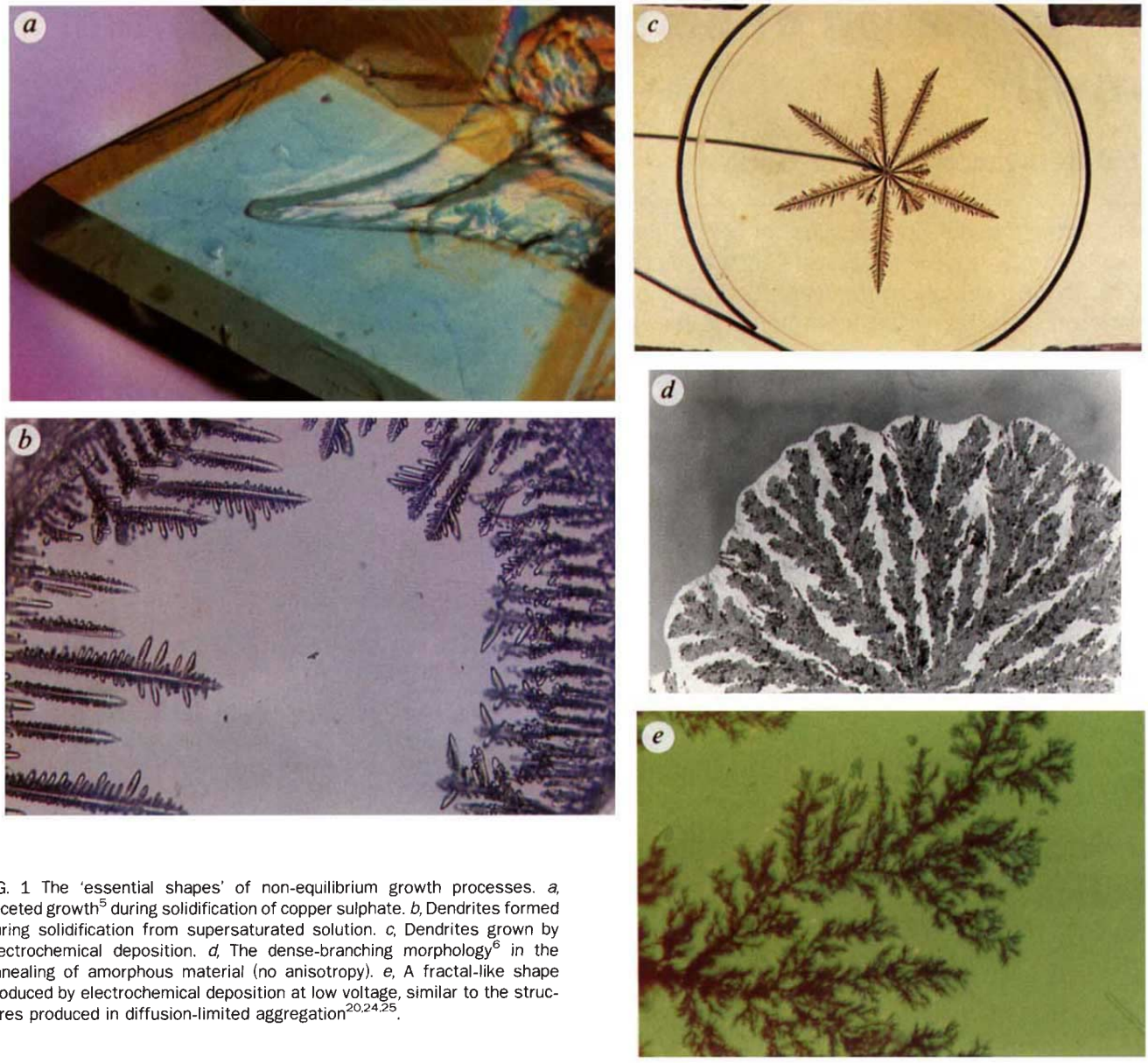

FIG. 1 The 'essential shapes' of non-equilibrium growth processes. *a*, Faceted growth[5] during solidification of copper sulphate. *b*, Dendrites formed during solidification from supersaturated solution. *c*, Dendrites grown by electrochemical deposition. *d*, The dense-branching morphology[6] in the annealing of amorphous material (no anisotropy). *e*, A fractal-like shape produced by electrochemical deposition at low voltage, similar to the structures produced in diffusion-limited aggregation[20,24,25].

The selection problem for dendritic growth

The principal problem that we try to resolve here is how microscopic dynamics, operative on the scale of ångströms, are amplified to such an extent that in a system out of equilibrium they control the macroscopic shape on a scale of centimetres. The natural inclination, however, is to strive for theories of growth that emphasize macroscopic dynamics and relegate the microscopic dynamics to a subsequent refinement; this was how the theory of dendritic growth initially evolved. Ivantsov showed[11] that for a solid forming from an undercooled melt, the propagating crystal front is parabolic when the process is controlled by heat diffusion alone (that is, when surface tension and surface kinetics are neglected). Both the parabolic shape of the tip and the predicted constant velocity are consistent with observations of dendritic growth. However, Ivantsov's solution specifies only the product of the dendrite tip's radius of curvature and its velocity; it cannot predict either one alone. Does this mean that dendrites with different tip curvatures and corresponding tip velocities, given by Ivantsov's criterion, coexist at a specified undercooling? Glicksman *et al.*[12] demonstrated that, for a given undercooling, only one dendrite (that is, one tip velocity and radius of curvature) is observed. This poses a 'selection problem'[4]: for given undercooling, the Ivantsov solution admits a continuous family of parabolic solutions, and yet for specified experimental conditions only one is seen. Moreover, it is known that these Ivantsov solutions are 'linearly unstable', meaning that they are unable to maintain their shape during growth[4].

The first attempts to resolve the stability problem were based on a hope that incorporation of surface tension would involve only a minor modification in shape of the Ivantsov parabolic fronts, while still producing stable solutions below a characteristic length scale. Oldfield[13] proposed that the selected dendrite was the one moving with the minimum speed (or maximum tip radius), which is stabilized by surface tension. Building on this idea, Langer and Müller-Krumbhaar[14] performed calculations to find this 'marginally stable' solution and further advanced the concept of such a selection principle.

A more complete incorporation of microscopic dynamics has had to await developments in computing and mathematical methods. The surprising result of these studies is that surface tension and surface kinetics are 'singular' perturbations in the dynamical equations for interface evolution, in the sense that

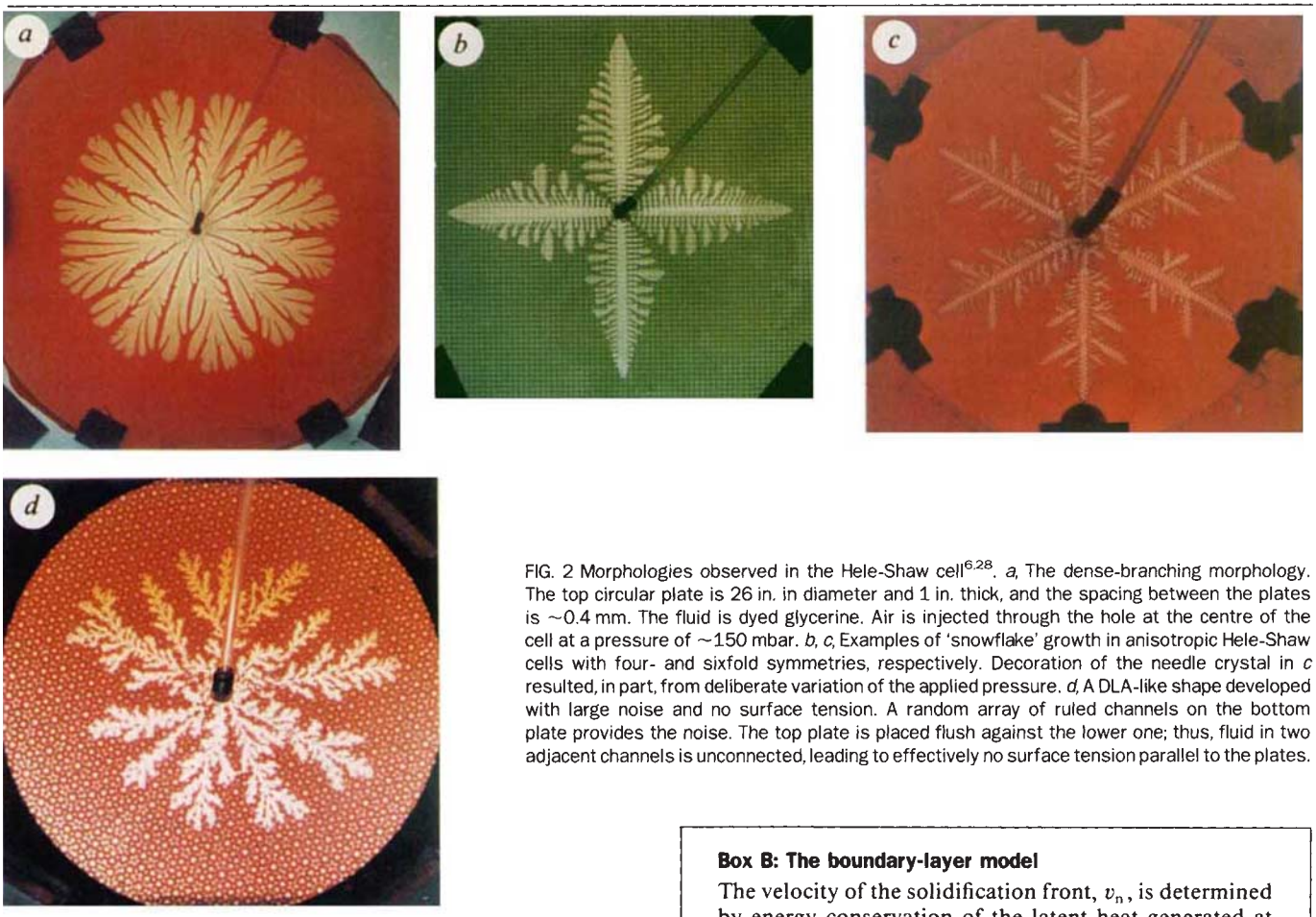

FIG. 2 Morphologies observed in the Hele-Shaw cell[6,28]. *a*, The dense-branching morphology. The top circular plate is 26 in. in diameter and 1 in. thick, and the spacing between the plates is ~0.4 mm. The fluid is dyed glycerine. Air is injected through the hole at the centre of the cell at a pressure of ~150 mbar. *b*, *c*, Examples of 'snowflake' growth in anisotropic Hele-Shaw cells with four- and sixfold symmetries, respectively. Decoration of the needle crystal in *c* resulted, in part, from deliberate variation of the applied pressure. *d*, A DLA-like shape developed with large noise and no surface tension. A random array of ruled channels on the bottom plate provides the noise. The top plate is placed flush against the lower one; thus, fluid in two adjacent channels is unconnected, leading to effectively no surface tension parallel to the plates.

they may totally alter the character of the solutions and so must be incorporated from the outset. Thus, the microscopic dynamics cannot be treated as small perturbations of macroscopic solutions; on the contrary, when microscopic dynamics are incorporated from the start, dendritic growth does not occur when surface tension and surface kinetics are isotropic. Instead, tip-splitting fingers develop, leading to the 'dense-branching morphology' discussed below. For dendritic growth, anisotropy is required in the interfacial dynamics[15].

The dense-branching morphology

The Hele-Shaw cell[16–19] provides a simple means of studying pattern formation. It consists of two closely spaced plexiglass plates sandwiching a layer of viscous fluid (we use dyed glycerine). The top plate is circular and open to the air at its edge. Through a tube at the centre of the plate a second, less viscous fluid (air or water) is injected to displace the glycerine.

Figure 2*a* shows an example of the dense-branching morphology (DBM) in the Hele-Shaw cell. It consists of fingers of well defined width confined within a roughly circular envelope. The splitting at the tip distinguishes the fingers from dendrites. This tip-splitting results from the interplay between the macroscopic diffusion field (corresponding to pressure in the Hele-Shaw cell), which tends to make the interface irregular, and the microscopic effects of isotropic surface tension and surface kinetics, which tend to keep the velocity uniform and the interface smooth. The velocity of a point on the interface in the direction normal to the interface is proportional to the pressure gradient at that point. If the less viscous fluid is air, for which the viscosity can be assumed to be zero, the pressure within the injected bubble is constant. In the more viscous fluid (here

Box B: The boundary-layer model

The velocity of the solidification front, v_n, is determined by energy conservation of the latent heat generated at the interface and its diffusion into the melt (ignoring heat diffusion in the solid): $v_n = -(DC_p/L)\nabla_n T$, where D is the thermal diffusion constant[4]. To calculate the velocity and predict the interfacial shape, the temperature throughout the melt must be known at all times. (The dynamics is nonlocal in both space and time because the interface is a free boundary.) For this full solidification (diffusion) problem, the diffusion equation $\partial T/\partial t = D\nabla^2 T$ must be solved with the boundary conditions that far away from the interface $T_\infty = T_m - \Delta$, where Δ is the undercooling and the interface temperature T_i (including microscopic effects) is described in Box A.

The boundary-layer model (BLM) simplifies the diffusion problem by assuming that the entire temperature change occurs within a narrow layer of width l, near the interface. In terms of l, the interface velocity is then $v_n = (DC_p/L)(T_i/l)$. We must now describe the time evolution of l, and this is done using a phenomenological approach. We define the heat content of the boundary layer per unit interfacial length, $H = C_p(T_i - T_\infty)l$. The time evolution of H is determined by heat balance within the boundary layer (along the normal direction) as the interface advances:

$$\left.\frac{dH}{dt}\right|_n = v_n L - C_p(T_i - T_\infty)v_n - \kappa v_n H + D\frac{\partial}{\partial s}\left(\frac{l\partial T_i}{\partial s}\right) \quad (1)$$

From left to right, the terms represent (1) the production of latent heat; (2) the heat needed to warm the next layer of melt to the surface temperature; (3) the change in heat owing to the increase in arc length, ds, along the interface; and (4) the change in heat resulting from the lateral diffusion of heat along the interface. Each interfacial point moves along the normal to the surface with velocity v_n.

glycerine) the pressure gradient is analogous to the concentration gradient in a very dilute solution at the boundary with a phase of different concentration. The pressure and concentration fields satisfy the Laplace equation[20]. In many physical cases the Laplace equation may be regarded as the 'infinite diffusion length' limit of the diffusion equation. The diffusion equation itself (see Box B) describes many examples of non-equilibrium growth: for example, solidification from an undercooled metal, precipitation from supersaturated solution or phase separation during amorphous annealing.

A key macroscopic effect of the pressure field at the interface is the diffusive (Mullins–Sekerka) instability[21], illustrated in Fig. 3*b*. We consider an interface that is initially circular but develops a bulge. The pressure gradient along the interface is greatest at the tip of the bulge because it is the closest point on the interface to the outer boundary (the local pressure gradient is the pressure drop between the interface and the boundary divided by the distance to the boundary). Because the velocity of a point on the interface is proportional to the local pressure gradient, the bulge grows faster than other parts of the interface. If this instability is the only mechanism acting, then noise or fluctuation in the diffusion field will cause the interface to break up into many growing bulges; these will develop smaller bulges, and so on *ad infinitum*. The result is an invasion of the more viscous phase by the less viscous one without ordering or a characteristic length scale. Experimental realizations of this situation are possible by making the interfacial tension very small, for example by using two miscible fluids[22] or by adding glass beads[23]. It is also the process that operates during diffusion-limited aggregation (DLA), in which case the diffusive instability leads to a fractal structure[7–9,20,24,25].

The microscopic effects of surface tension and surface kinetics compete with the diffusive instability. Surface tension acts to reduce the pressure at the highly curved parts of an interface, and surface kinetics reduce the pressure on the faster-moving portions (see Box A). In Fig. 3*c* we show the calculated rate of growth or decay of small-amplitude perturbations imposed on the interface, with these effects incorporated (a 'linear stability analysis'[6,26,27]). For simplicity, we consider wave perturbations (Fig. 3*b*) characterized by the mode number m, the number of waves that fit on the interface. The effects of surface tension and surface kinetics are seen to be too weak to stabilize a circular interface.

Linear stability analysis can be used to investigate the branching rate of the fingers, which may be the best way to characterize the DBM. This branching rate can be studied by finger counting or by Fourier analysis. Figure 3*c* shows that there is a fastest growing perturbation, with mode number m^*, which produces an interface modulated by m^* finger-like bulges. The value of m^* is determined by the pressure gradient across the system and the surface parameters. As a finger develops, the pressure at the tip is reduced by surface tension and surface kinetics, slowing it down. The finger flattens and eventually splits. It is natural to expect, and has been found experimentally[6,26], that the rate of tip-splitting is such that the number of fingers can be approximated by m^*. Hence m^* embodies the characteristic length scale of the DBM, and reflects the competition between the diffusive instability and microscopic effects[28].

The circular envelope of the DBM (observed with circular boundary conditions) is an integral part of the dynamics of the pattern. A naive understanding of how it arises is that if one finger outgrows the others it has more space to spread out; part

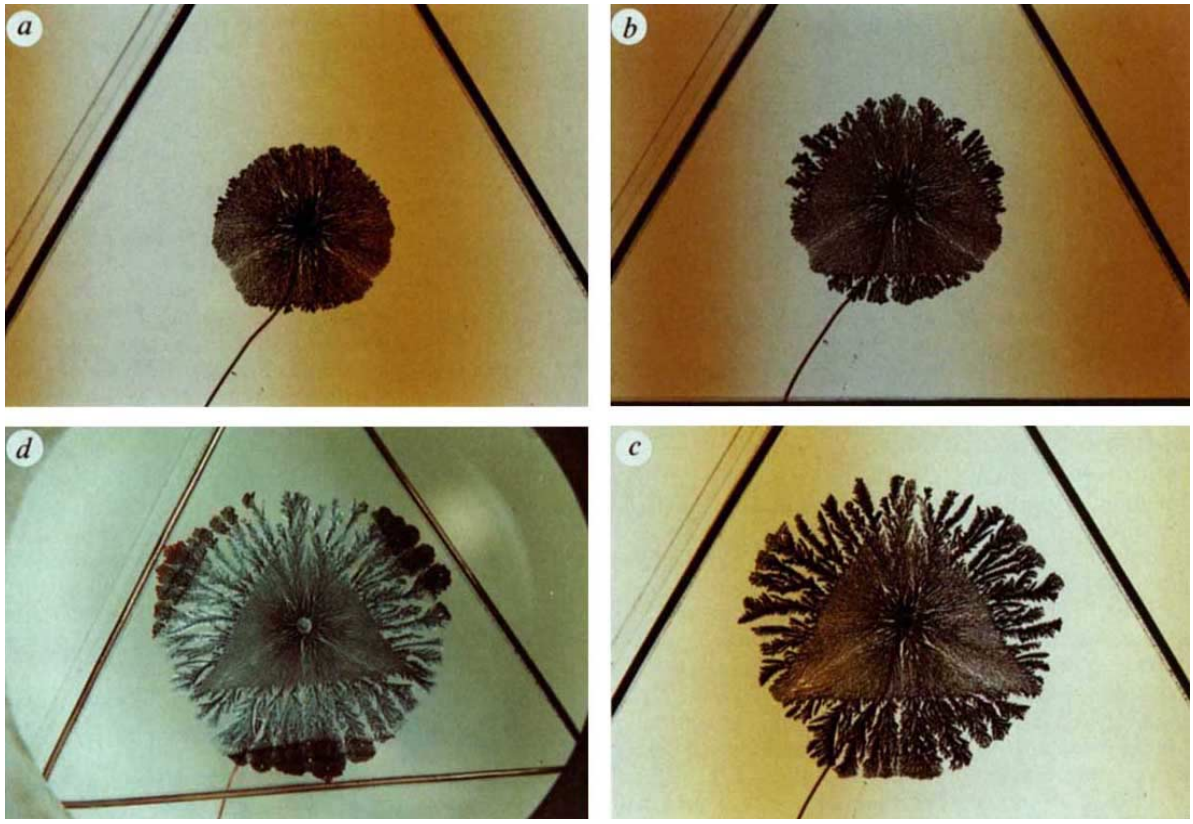

FIG. 6 Morphology transition in electrochemical deposition of zinc from 0.05M $ZnSO_4$ solution between plexiglass plates spaced about 0.3 mm apart[36]. The outer anode has a triagonal shape (8 cm edge). The first transition ($a \rightarrow b$) is from tip-splitting growth to dendritic growth. The change in colour reflects the change in the microscopic structure of the two morphologies. The second transition ($c \rightarrow d$) is due to the effect of the copper ions from the outer electrode affecting the microstructure of the deposit. Transitions between two dense-branching morphologies with different branch densities are also observed in electrochemical deposition of copper[51].

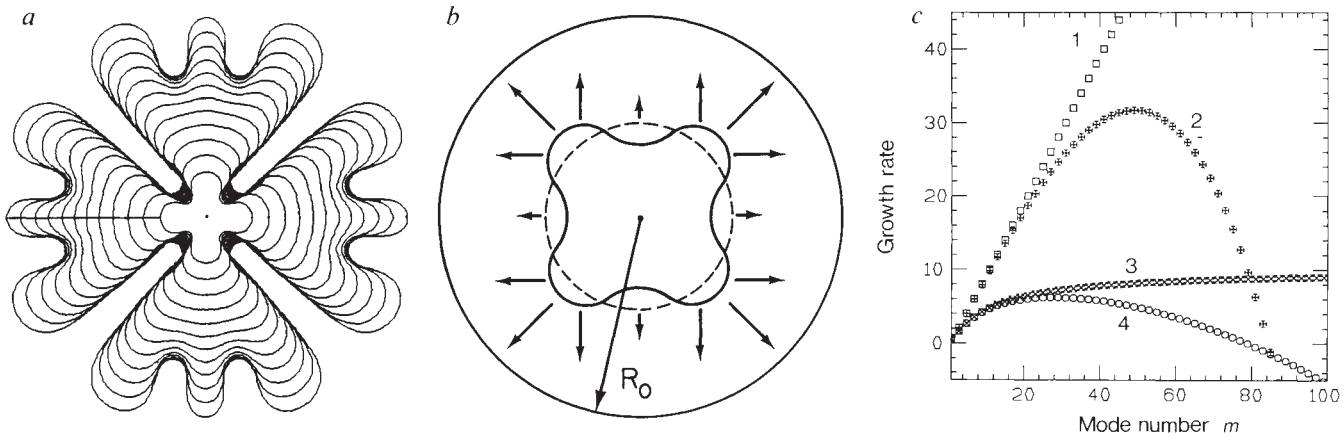

FIG. 3 The DBM and linear stability analysis. *a*, Computer simulation of the time evolution of an isotropic Hele-Shaw cell experiment, showing two cascades of tip-splitting[50]. *b*, Schematic illustration of the Mullins–Sekerka instability[21]. The solid curve is a fourfold deformation ($m=4$) of a circular interface (dashed line). The four bulges are closer to the outer boundary (circle with radius R_0), so the pressure gradient and the velocity (arrows) is larger at their tips. *c*, Results of the linear stability analysis, showing the initial growth rate as a function of the mode number m for sinusoidal perturbations of a circular interface. Line 1 is for constant pressure along the interface without surface tension or surface kinetics; line 2 is with surface tension included; line 3 is with surface kinetics; and line 4 is with both surface tension and surface kinetics. In the first case there is no fastest-growing mode.

of the flow goes sideways and the finger flattens and slows down. We believe that a nonlinear analysis will be required to understand the growth of this envelope. Recently, a linear stability analysis was proposed to explain the DBM as seen during electrochemical deposition[29].

Experiments indicate that, in the absence of pronounced anisotropy, tip-splitting is the generic mode of growth; it is observed, for example, in growth by electrochemical deposition[30,31], precipitation from supersaturated solution, solidification from undercooled melts[32], amorphous annealing[6] and spherulitic growth[33]. The most pressing unsolved problem is the determination of the branching rates[34,35] and velocity[28,33,36] of DBM growth. The latter is especially intriguing because a selection mechanism may operate to give a constant interfacial velocity.

Anisotropy and dendritic growth

The Hele-Shaw cell can also be used to study anisotropic growth, which is analogous to the solidification of a crystalline material. Crystalline anisotropy may be mimicked very simply in the cell by engraving channels on one of the plates[37]. The fluid velocity is proportional to the square of the plate spacing; because channels modulate the spacing between the plates, the directions along the channels become the preferred growth directions. With an engraved lattice of sixfold symmetry (three sets of parallel channels oriented at 120° to each other), the air bubble adopts shapes reminiscent of snowflakes, with six dendritic arms. (Because snowfall on Mars is composed of CO_2 flakes with fourfold anisotropy, lattices with fourfold symmetry mimic 'Martian snowflakes'.) The formation of dendrites in the

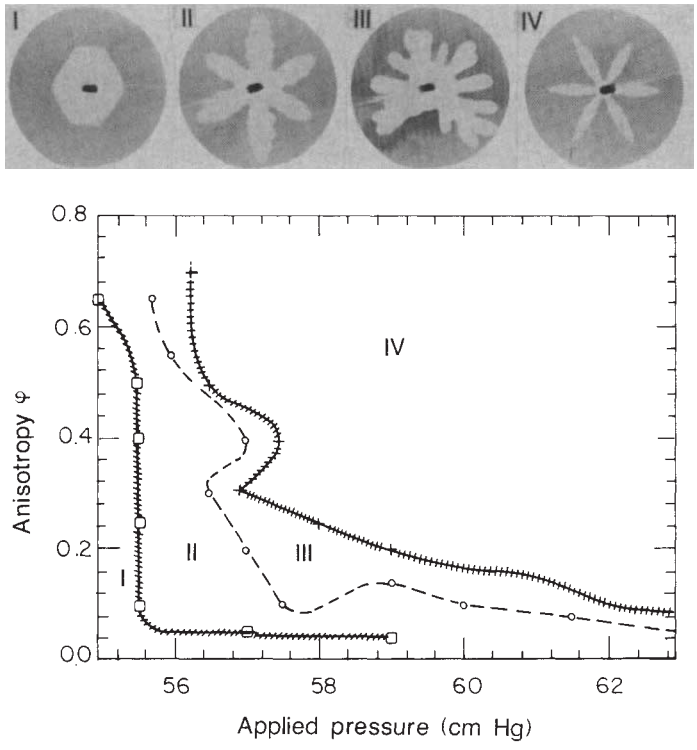

FIG. 4 Morphology diagram for a sixfold anisotropic Hele-Shaw cell[28,37]. The anisotropy of the cell is quantified by the ratio $\phi = b_1/(b_0+b_1)$, where b_1 is the depth of the grooves (0.015 in.), and b_0 is the spacing between the top plate and the top of the grooved plate. The morphology regions are: (I) faceted growth; (II) surface-tension dendritic growth (the dendrites are inclined at an angle of 30° to the grooves); (III) tip-splitting growth; and (IV) kinetic dendritic growth (the dendrites grow parallel to the grooves). Cross-hatching on morphology boundaries indicates the possible existence of narrow regions of other morphologies. (For more details see ref. 28). At pressures between regions (II) and (IV), the anisotropies of surface tension and surface kinetics are of comparable strength and cancel each other, leading to vanishing effective anisotropy and thus to tip-splitting growth.

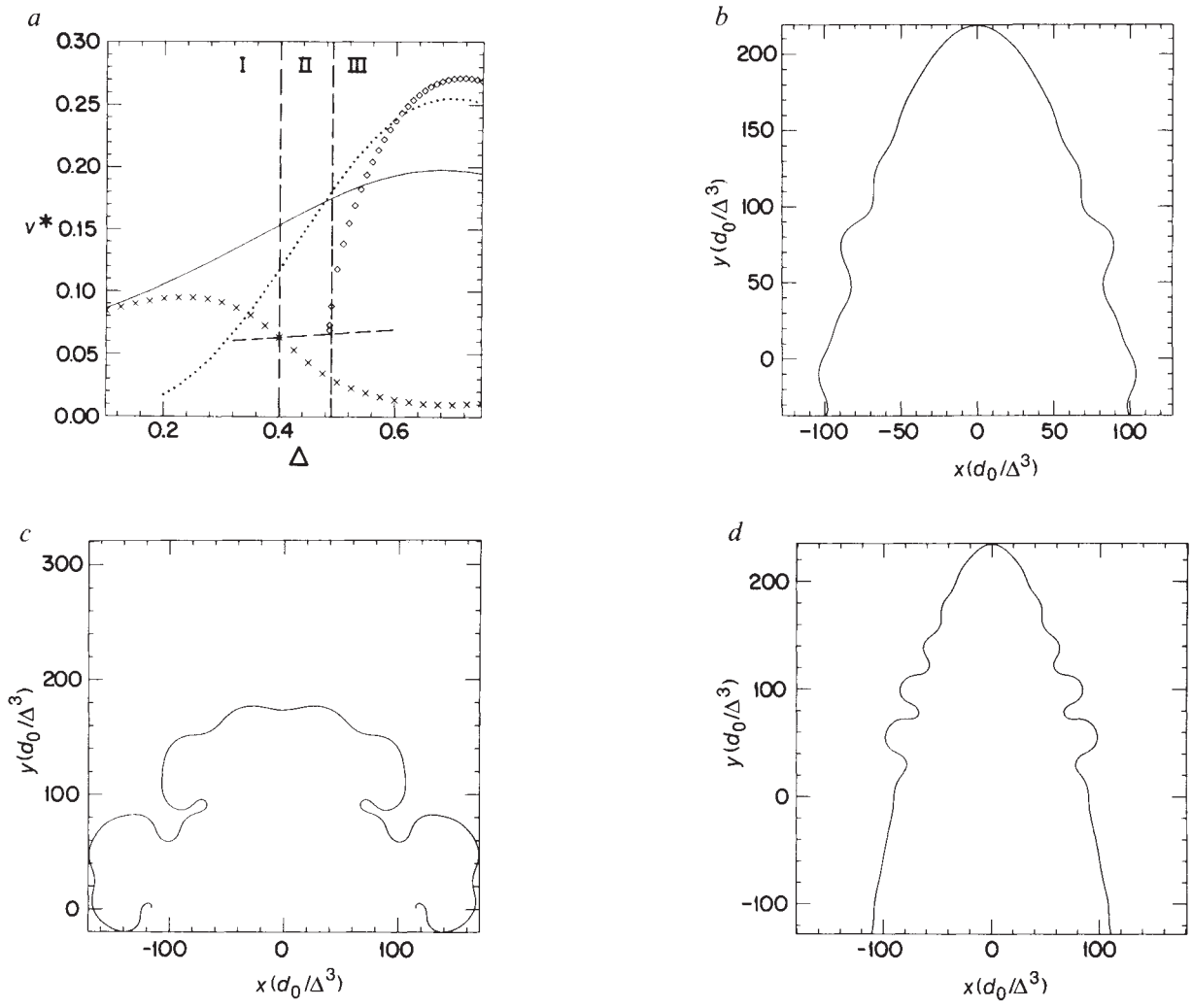

FIG. 5 *a*, The morphology diagram and the needle-crystal selected velocity v^* (dimensionless units) for competing anisotropies in the BLM[28]. Surface-tension and surface-kinetics anisotropies have preferred growth directions offset by 30°, as in the sixfold Hele-Shaw cell. Crosses indicate the selected velocity of needle crystals pointing in the preferred direction of the surface-tension anisotropy, and diamonds are for crystals pointing in the surface-kinetics preferred direction. The nearly horizontal dashed line represents our calculation of the DBM velocity. The solid line is the selected velocity for the 'surface-tension' needle crystal in the absence of kinetic anisotropy, and the dotted line is that for the 'kinetic' needle crystal with no surface-tension anisotropy. *b*, Time-dependent simulation of a surface-tension dendrite in regime I; *c*, Tip-splitting growth in regime II; and *d*, surface-kinetic dendrite in regime III. Above a critical undercooling Δ_c, surface-kinetics dendrites have the higher growth velocity and are the observed morphology. There is a discontinuous jump in the velocity at Δ_c, indicating a first-order transition from the DBM to surface-kinetics dendrites. The transition from surface-tension dendrites to the DBM is second order.

Hele-Shaw cell[37] provides a graphic demonstration of the role of anisotropy in dendritic growth.

As the applied pressure (the driving force) is varied, the air bubble assumes other shapes. Similarly, as the 'microscopic' conditions are altered, different morphologies emerge. For example, the 'strength' of anisotropy can be changed by varying the spacing between the plates. One can devise a 'morphology diagram' to organize these observations[28]. Figure 4 depicts a morphology diagram for a cell with sixfold anisotropy. For different values of the applied pressure, one may obtain faceted growth, the DBM or two types of dendrites. As explained below, the existence of two different types of dendrites is particularly significant in an understanding of morphology transitions. Morphology diagrams have also been formulated for electrochemical deposition experiments[30,31], Hele-Shaw cells using liquid crystals as the viscous fluid[26], and solidification from supersaturated solutions[37].

Several questions now arise. When does anisotropy trigger dendritic rather than tip-splitting growth? What is the difference between the dendrites appearing close to equilibrium and those far from equilibrium? Is there a general principle that allows one to predict the mode of growth for specified conditions from the available morphologies, and thus to explain the morphology diagram?

We can construct an heuristic, albeit far from definitive, argument to understand the selection of tip-splitting or dendritic growth, and the role of anisotropy. Consider a crystal solidifying with a parabolic interface and a finite surface tension. The tip is the coldest point on the interface (see Box A). Thus there is a heat gradient along the interface, and heat flows towards the tip. This warming slows the advance of the interface, while the corresponding cooling of points at the sides of the tip causes these points to advance faster and to overtake the tip. Such interfacial heat-balance dynamics probably accounts for tip-splitting growth. For dendrites to form, heat flow towards the tip must be suppressed; this happens in the presence of crystalline anisotropy. For large enough anisotropy (of the order of one part in a hundred), the tip is no longer the coldest point along the interface, and a subtle interplay may develop between the anisotropy and the shape selection of the needle crystal. For

Box C: Microscopic solvability criterion

We seek steady-state (constant-velocity and shape-preserving) solutions of the BLM with a needle-crystal-like shape[39,40]. If an interface advancing in the $\theta = 0$ (ordinate) direction with constant velocity v_0 preserves its shape, then the interface velocity in the normal direction is $v_n = v_0 \cos\theta$, and in the tangential direction is $v_t = v_0 \sin\theta$. The properties of the boundary layer are stationary in the moving frame: in other words, the time derivative of H at fixed arclength vanishes. That is,

$$\left.\frac{dH}{dt}\right|_s \equiv \left.\frac{dH}{dt}\right|_n - \left(\frac{\partial H}{\partial s}\right) v_t = 0 \qquad (2)$$

and the derivative along the normal direction is equation (1) (Box B). In the absence of surface tension and surface kinetics, the interfacial temperature is constant, $T_i = T_m$, and equation (1) can be solved exactly. For a given value of undercooling there exists a continuous family of parabolic Ivantsov-like solutions. The singular nature of surface effects manifests itself in the fact that these solutions are destroyed when either surface tension or surface kinetics are included. These singular perturbations change completely the nature of the solution and lead to tip-splitting rather than needle-crystal growth. Anisotropy is also a singular perturbation. The surprising discovery is that when it is included needle-crystal-like solutions are recovered.

To demonstrate the existence of such solutions, equation (2) is rewritten as three first-order coupled nonlinear differential equations[40]. These equations describe a 'flow' in the three-dimensional space whose coordinates are θ, T_i and $\lambda = dT_i/ds$. There are two special fixed points: $(d\theta/ds = dT_i/ds = d\lambda/ds = 0)$ at $\theta = \pm\pi/2$, $T_i = T_m$ and $\lambda = 0$. A needle-crystal solution is a trajectory connecting these two fixed points. The problem is posed in terms of $\lambda(s = 0)$, the 'mismatch function'. Because the temperature must be symmetric about the origin ($s = 0$, $\theta = 0$), the mismatch function must vanish for an eigenvalue v_0 if a needle crystal is to exist. In the absence of anisotropy there is no selected needle crystal. But for any finite level of anisotropy there is a discrete set of eigenvalues, $\{v_0\}$, for which the mismatch function vanishes. The phrase 'microscopic solvability' reflects the subtle interplay, in the determination of these eigenvalues, between the macroscopic driving force of the undercooling and microscopic interfacial effects.

a given anisotropy, only a needle crystal with a particular tip velocity and curvature will have its coldest point at the appropriate temperature and distance from the tip to exactly balance the tip-splitting tendency. This is the origin of the 'solvability' criterion (Box C). It is found that, instead of the original (Ivantsov) continuous family of parabolas, only a discrete set of (nearly parabolic) needle-crystal solutions can satisfy this criterion. A stability argument is required to select one solution from this discrete set. If a needle crystal is perturbed, say by introducing a bulge near the tip, the perturbation will grow as a result of the diffusive instability. This bulge grows outwards at a fixed position in space, so as the tip advances the bulge moves backwards relative to the tip. Only for the fastest-growing needle crystal does the bulge move backwards faster than its growth rate, allowing the tip to regain its original shape. Thus, only the fastest growing needle crystal can survive the effect of the diffusive instability.

This microscopic solvability criterion was discovered independently using the geometrical[39] and boundary-layer[40] models. It has since been shown that the same mechanism is present in the full solidification problem, and analytical methods have been developed to calculate the selected velocity in the limit of small undercooling and small anisotropy[41–43]. There is good agreement with time-dependent supercomputer simulations of the full solidification problem[44]; the selection hypothesis is, however, yet to be tested comprehensively against experiment.

A complete theory of dendritic growth must also explain the dynamic development of side branches. Much attention is being given to this question[45–48]; the debate focuses on the relative roles of noise and deterministic dynamics. The question is whether side branches grow as a result of noise that triggers a diffusive instability (such that a linear stability analysis would be sufficient to predict their evolution) or whether, as we believe, an additional solvability principle is required.

Selection hypothesis for morphology transitions

With the discovery of the microscopic solvability criterion outlined in Box C, the problem of dendritic growth seemed to be solved. But the anisotropic Hele-Shaw experiment and the boundary-layer model (BLM) (see Box C) expose a problem: dendrites are not always observed when anisotropy is present. As the driving force (pressure in the Hele-Shaw cell and undercooling in the BLM) is decreased, tip-splitting occurs below a critical value. (Similar behaviour is observed experimentally in the solidification of water[32].) The selection principle for dendritic growth, however, predicts that whenever anisotropy is present, a specific dendrite (corresponding to the fastest-growing needle crystal) exists and is linearly stable. The observation of tip-splitting under growth conditions appropriate to dendrites raises the possibility that morphologies can coexist. As only one morphology is selected experimentally, microscopic solvability must be incomplete—a more general principle is needed.

A plausible extension of the solvability criterion is the more general principle that the dynamically selected morphology is the fastest-growing one[28]. That is, if more than one morphology is possible, only the fastest one is nonlinearly stable and hence observable. Thus, we infer that below a critcal driving force the velocity of the DBM is greater than the velocity of the dendritic solution predicted for the same parameters, and so the former is selected. To test this hypothesis, we have studied the effect of competing anisotropies using the BLM. We included anisotropies in both surface tension and surface kinetics, with preferred growth directions offset by 30°. The results for the selected velocity along both the surface-tension and surface-kinetics directions (Fig. 5) show that above a critical undercooling both types of dendrites are possible, but those with highest velocity are controlled by the surface kinetics. Time-dependent simulations of the BLM demonstrate that the 'surface-kinetics' dendrites do indeed comprise the dynamically selected morphology in this regime. Further studies of experimental systems and comparison with theoretical models are required to test this 'fastest-growing' selection hypothesis.

An analogy can be drawn between phase diagrams and morphology diagrams. At equilibrium, the phase that minimizes the free energy, for a given set of state variables, is the selected one, irrespective of the prior history of the system. By contrast, non-equilibrium growth processes are time dependent, so it is not clear *a priori* that a morphology diagram can exist. The question is whether appropriate control parameters describing the growth conditions, analogous to the state variables of thermodynamics, can be identified such that the morphology depends only on these parameters and not on initial conditions. One finds that morphology diagrams can indeed be mapped out for experimental systems, and are reproducible as a function of the control parameters. It follows that a corresponding selection principle, which would permit theoretical prediction of growth morphologies, must exist.

The analogy between equilibrium phase diagrams and morphology diagrams can be carried further. Two types of morphology transition can be identified[28]: the first shows a

discontinuous jump in the velocity at the transition point (and is hence classified as a first-order morphology transition), whereas for the other (characterized as second-order), the velocity itself is continuous as the morphology changes but there is a discontinuity in its derivative. Such morphology transitions are found both experimentally and theoretically. In a study of solidification from supersaturated NH_4Cl solutions, Chan *et al.*[37] found that there was either a jump discontinuity (first order) or a discontinuity in the slope (second order) of the observed dendritic velocity as a function of supersaturation, corresponding to changes in crystallographic orientation of the growing dendrites. First- and second-order morphology transitions in the BLM are shown in Fig. 5.

Experiments on growth by electrochemical deposition produce results that are in qualitative agreement with this characterization of morphology transitions. Sawada *et al.*[30] have plotted the interfacial velocity against applied voltage and found sudden changes in slope when the morphology changes. We have observed discontinuities in both slope and magnitude of the interfacial velocity, depending on the growth parameters. The morphology transition in electrochemical deposition shown in Fig. 6 demonstrates two key aspects of such transitions: the transition is sharp and is accompanied by a change in the microstructure of the growing deposit (in this case coincident with a colour change). These observations lend support to the concept of morphology transitions.

Concluding remarks

The existence of a morphology diagram indicates that a selection principle must exist. Is this principle the 'fastest-growing morphology' hypothesis that we have proposed? We believe that this may not be the most general principle but is at least a step in the right direction.

When a system is driven out of equilibrium by the imposition of a gradient in one of the thermodynamic variables (such as the temperature or the concentration), the response of the system is described by the conjugate flux (the heat flux and particle flux, respectively). These fluxes may in general be viewed as the rate of entropy production, or the rate of approach towards global equilibrium. In growth processes specifically, the driving force (for example, the undercooling in solidification) is the equivalent of the thermodynamic gradient. The average velocity measures the rate of approach towards equilibrium, and therefore represents a response function. But the global rate of change of the free energy (at the interface) is given by the integral of the velocity along the interface. Thus, by 'average velocity' we mean the velocity weighted according to the geometry of the interface, and thus we take into account the global shape of the object. We speculate that the average velocity is an important variable but is by no means the only one. It should have a conjugate variable (at present unknown) that will be characteristic of the equilibrium properties of the interface and the selected growth morphology.

The 'fastest-growing' selection principle is probably a good approximation to the general selection principle when the system is far from equilibrium, in which case the growth rate is the dominant factor in the competition between morphologies. An analogy can be drawn with the high-temperature limit of an equilibrium system coupled to a heat bath, where entropy is dominant: thus, we expect that far from equilibrium, entropy production is dominant in morphology selection. □

Eshel Ben-Jacob and Peter Garik are in the Department of Physics, University of Michigan, Ann Arbor, Michigan 48109, USA, and the School of Physics and Astronomy, Tel Aviv University, 69978 Tel Aviv, Israel.

1. Kepler, J. *De Nive Sexangula Godfrey Tampach* (Frankfurt am Main, 1611).
2. Thompson, D. W. *On Growth and Form* (Cambridge University Press, 1944).
3. Fife, P. C. *Mathematical Aspects of Reacting and Diffusing Systems* (Springer, New York, 1979).
4. Langer, J. S. *Rev. mod. Phys.* **52,** 1–28 (1980).
5. Woodruff, D. P. *The Solid-Liquid Interface* (Cambridge University Press, 1973).
6. Ben-Jacob, E., Deutscher, G., Garik, P., Goldenfeld, N. D. & Lereah, Y. *Phys. Rev. Lett.* **57,** 1903–1906 (1986).
7. Pietronero, L. & Toscotti, E. (eds) *Fractals in Physics* (North Holland, Amsterdam, 1985).
8. Feder, J. *Fractals* (Plenum, New York, 1988).
9. Vicsek, T. (ed.) *Fractal Growth Phenomena* (World Scientific, New York, 1989).
10. Nakaya, U. *Snow Crystals* (Harvard University Press, 1954).
11. Ivantsov, G. P. *Dokl. Akad. Nauk. SSSR* **58,** 567–569 (1947).
12. Glicksman, M. E., Shaefer, R. J. & Ayers, J. D. *Metall. Trans.* A**7,** 1747–1759 (1976).
13. Oldfield, W. *Mater. Sci. Engng* **11,** 211–218 (1973).
14. Langer, J. S. & Muller-Krümbhaar, H. *Acta metall.* **26,** 1681–1687 (1978); **26,** 1689–1695 (1978); **26,** 1697–1708 (1978).
15. Ben-Jacob, E., Goldenfeld, N. D., Langer, J. S. & Schön, G. *Physica* D**12,** 245–252 (1984); *Phys. Rev. Lett.* **51,** 1930–1932 (1983); *Phys. Rev.* A**29,** 330–340 (1984).
16. Hele-Shaw, H. S. *Nature* **58,** 34–36 (1898).
17. Paterson, L. *J. Fluid Mech.* **113,** 513–529 (1981); *Phys. Rev. Lett.* **52,** 1621–1625 (1984).
18. Maher, J. V. *Phys. Rev. Lett.* **54,** 1498–1501 (1985).
19. Bensimon, D., Kadanoff, L. P., Liang, S., Shraiman, B. I. & Tang, C. *Rev. mod. Phys.* **58,** 977–999 (1986).
20. Sander, L. M. *Nature* **322,** 789–793 (1986).
21. Mullins, W. W. & Sekerka, R. F. *J. appl. Phys.* **34,** 323–329 (1963); **35,** 444–451 (1964).
22. Nittman, J., Daccord, G. & Stanley, H. E. *Nature* **314,** 141–144 (1985).
23. Måløy, K. J., Feder, J. & Jossang, J. *Phys. Rev. Lett.* **55,** 2681–2684 (1985).
24. Witten, T. A. & Sander, L. M. *Phys. Rev. Lett.* **47,** 1400–1403 (1981); *Phys. Rev.* B**27,** 5686–5697 (1983).
25. Meakin, P. *Phys. Rev.* A**27,** 604–607 (1983); A**27,** 1495–1507 (1983).
26. Buka, A. & Palffy-Muhoray, P. *Phys. Rev.* A**36,** 1527–1529 (1987).
27. Schwartz, L. *Phys. Fluids* **29,** 3086–3088 (1986).
28. Ben-Jacob, E., Garik, P., Mueller, T. & Grier, D. *Phys. Rev.* A**38,** 1370–1380 (1988).
29. Grier, D., Kessler, D. A. & Sander, L. M. *Phys. Rev. Lett.* **59,** 2315–2318 (1987).
30. Sawada, Y., Dougherty, A. & Gollub, J. P. *Phys. Rev. Lett.* **56,** 1260–1263 (1986).
31. Grier, D., Ben-Jacob, E., Clarke, R. & Sander, L. M. *Phys. Rev. Lett.* **56,** 1264–1267 (1986).
32. Tirmizi, S. H. & Gill, W. N. *J. Cryst. Growth* **96,** 277–292 (1989).
33. Goldenfeld, N. D. *J. Cryst. Growth* **84,** 601–608 (1987).
34. May, S. E. & Maher, J. V. *Phys. Rev.* A**40,** 1723–1726 (1989).
35. Sarkar, S. & Jasnow, D. *Phys. Rev.* A**39,** 5299–5307 (1989).
36. Garik, P. *et al. Phys. Rev. Lett.* **62,** 2703–2706 (1989).
37. Ben-Jacob, E. *et al. Phys. Rev. Lett.* **55,** 1315–1318 (1985).
38. Chan, S. K., Reimer, H. H. & Kahlweit, M. *J. Cryst. Growth* **32,** 303–315 (1976).
39. Kessler, D. A., Koplik, J. & Levine, H. *Phys. Rev.* A**30,** 3161–3174 (1984).
40. Ben-Jacob, E., Goldenfeld, N. D., Kotliar, B. G. & Langer, J. S. *Phys. Rev. Lett.* **53,** 2110–2113 (1984).
41. Kessler, D. A., Koplik, J. & Levine, H. *Adv. Phys.* **37,** 255–339.
42. Langer, J. S. in *Chance and Matter* Les Houches Summer School (eds Souletie, J., Vannimenus, J. & Stora, R.) (1987).
43. Langer, J. S. *Science* **243,** 1150–1155 (1989).
44. Saito, Y., Goldbeck-Wood, G. & Muller-Krumbhaar, H. *Phys. Rev. Lett.* **58,** 1541–1544 (1987).
45. Dougherty, A., Kaplan, P. D. & Gollub, J. P. *Phys. Rev. Lett.* **58,** 652–658 (1987); *Phys. Rev.* A**38,** 3043–3053 (1988).
46. Pieters, R. & Langer, J. S. *Phys. Rev. Lett.* **56,** 1948–1951 (1987).
47. Barber, M., Barbieri, A. & Langer, J. S. *Phys. Rev.* A**36,** 3340–3349 (1987).
48. Martin, O. & Goldenfeld, N. *Phys. Rev.* A**35,** 1382–1390 (1987).
49. Raz, E., Lipson, S. G. & Polturek, E. *Phys. Rev.* A**40,** 1088–1095 (1989).
50. Sander, L. M., Ramanlal, P. & Ben-Jacob, E. *Phys. Rev.* A**32,** 3160–3163 (1985).
51. Hecker, N. thesis, Univ. of Michigan (1988).

ACKNOWLEDGEMENTS. We thank K. Mullen and M. Ben-Jacob for their assistance in preparing the manuscript. We thank A. Ben-Jacob, Y. Lereah and P. Ramanlal for some of the figures. This work was supported by the Petroleum Research Fund administered by the American Chemical Society, the German Israel Foundation, and the US National Science Foundation.